https://doi.org/10.1016/j.intermet.2013.11.020 This is the Pre-Published Version.

Diffusion bonding of a Zr-based metallic glass in its supercooled liquid region

J.G. Wang[a,b], J.C. Fan[b], Y.F. Zhang[c], G. Wang[d], W.H. Wang[e], K.C. Chan[a,*]

[a]Advanced Manufacturing Technology Research Centre, Department of Industrial and Systems Engineering, The Hong Kong Polytechnic University, Hung Hom, Hong Kong

[b]School of Materials Science and Engineering, Anhui University of Technology, Ma'anshan 243002, China

[c]Institute of Microstructure and Property of Advanced Materials, Beijing University of Technology, Beijing 100022, China

[d]Laboratory for Microstructures, Shanghai University, Shanghai 200444, China

[e]Institue of Physics, Chinese Academy of Sciences, Beijing 100190, China

*Electronic mail: kc.chan@polyu.edu.hk

Abstract

Based on the analyses of the influences of temperature and pressure on diffusion behavior with time, a Zr-based bulk metallic glass is successfully bonded in its supercooled liquid region. The temperature is found to be a key factor for the success of the bonding process if sufficient pressure and time are adopted. Three-point bending tests show that the flexural performance of the samples bonded with various parameters is significantly different. The parameters in favor of diffusion bonding do not automatically benefit the performance of the bonded materials. Diffusion makes the nano-voids shrink to form metallurgical bonding at the interface and it causes structural relaxation leading to the embrittlement inside bulk. Balance between the two aspects is the key to the bonding success and the utility of the bonded materials.

Keywords: B. Glass, metallic; C. Diffusion-bonding; F. Mechanical testing

1. Introduction

Since the metallic glass (MG) was first reported in 1960 [1], extensive efforts have been made to explore their fabrication, properties and applications [2-5]. In the 1970s, continuous and uniform MG ribbon with a thickness of tens of microns was produced by the melt-spinning method [6]. The ribbon is very flexible and can undergo 180^o bending without fracture due to the geometric effect [7], though the bulk glassy material is usually brittle at room temperature. For outstanding flexibility, Fe-based glass ribbon with excellent magnetic properties was conveniently wound to the core of a power transformer and has been extensively employed in the electrical industry [8]. When the MGs with characteristic specimen sizes in excess of 1 mm, so-called bulk metallic glasses (BMGs), were fabricated and tested, it was found that they were universally brittle and often fractured in a catastrophic manner at room temperature despite high strength [9]. The brittleness does a great harm to the processability of BMGs, and makes it impossible to die-stamp BMGs into components like aluminum or steel. Fortunately, there is a supercooled liquid region (SCLR) between the glass transition temperature (T_g) and the crystallization temperature (T_x) in MGs. In the SCLR, the undercooled liquids of metals have viscosities down to ~10^5 Pa·s, depending on their fragility and the absolute temperature, so they can be thermoplastically processed to net-shape hardware through blow or injection molding [4,10]. However, the time window for processing is restricted, because the supercooled liquid is metastable and it will relax and then crystallize during the heating and temperature holding procedures [2]. This demands the hardware to be simple and small so that the processing is completed within a short time. For the hardware with complex and big geometries, direct molding is no longer able to meet the design requirements alone.

Over the past years, welding and bonding have been introduced to integrate individual parts of BMGs into a unit [11-12]. A series of BMGs have been successfully joined in the liquid phase or supercooled liquid phase. Typically, pulse current, electron beam and laser joining are forms of liquid phase bonding [11]. However, this type of joining is implemented at a temperature above the melting point of the alloy, so the weld must be subsequently cooled fast enough to avoid crystallization of the material in the heat-affected zone. For BMGs with ordinary

liquid stability, to keep the glassy nature of the weld bead is difficult. In laser welding on a $Zr_{55}Al_{10}Ni_5Cu_{30}$ BMG with a critical casting thickness of 30 mm, Kawahito et al. [13] found that the weld bead devitrified even though the welding speed was 45 m/min, about two orders of magnitude larger than commercially possible. Generally, the intermetallic compounds precipitated in the BMG matrix are brittle, and sometimes result in microcracks due to the volume contraction, thereby affecting the performance of BMGs in a detrimental way [14]. Therefore, supercooled liquid phase bonding, or diffusion bonding (DB) in SCLR, was developed, in which the critical cooling rate for the maintenance of the glassy state of the bonded BMGs is relatively slower owing to the lower operating temperature [12]. Kuo et al. joined similar and dissimilar BMGs in their SCLRs, but the crystalline phase was still detected at the bonding interface in $Zr_{47.5}Cu_{47.5}Al_5$ with micro-focus X-ray diffraction [15]. In the DB of $Zr_{65}Al_{10}Ni_{10}Cu_{15}$ [12], crystallization was excluded, but the lap shear strength of the bonded sample was only 20% of that of the as-cast one. This indicates that the underlying mechanism for the DB of BMGs is not fully understood and the parameters for the DB are yet to be optimized. In this work, the DB mechanism for a Zr-based BMG is investigated. Various temperatures, pressures and times for DB are attempted, and their interrelationships are analyzed, and the flexural performance of the bonded specimens examined.

2. Experimental Procedures

2.1 Diffusion bonding and three-point bending

A Zr-based BMG with a chemical composition of $Zr_{52.5}Al_{10}Cu_{15}Ni_{10}Be_{12.5}$ (at.%) is used because of its wide SCLR of 129 ^oC (Tg ~ 416 ^oC and Tx ~ 545 ^oC) [16] which means a strong resistance to crystallization. BMG sheets of dimensions 20 mm × 5 mm × 1 mm are polished with abrasive paper and their glass state is ascertained by x-ray diffraction (XRD). Before bonding, the time-temperature-transformation (TTT) diagram is roughly measured by isothermal annealing at different temperatures using differential scanning calorimetry (DSC) at a heating rate of 40 K/min. Then for

each bonding experiment, every two sheets are stacked and loaded in a vacuum chamber at 10^{-2} Pa, followed by heating at a rate of 40 K/min to the bonding temperature as monitored by a thermocouple. The bonding setup is schematically shown in Fig.1. The sample is loaded for 10 or 15 minutes at a certain bonding temperature, and then cooled by power turn-off and introduction of Ar gas into the chamber. The successfully bonded samples are three-point bended at room temperature using an Instron test system with support span of 8 mm and displacement control of 0.1 mm/min. The rupture behavior is investigated by SEM.

2.2 Selection of DB parameters

DB, frequently combined with superplastic forming (SPF), is usually used for the fabrication of titanium (e.g. Ti-6Al-4V) aerospace components [17]. In general, there are three main parameters that govern the DB process, viz., temperature, pressure and time. The selection of the bonding temperature is considered as the primary decision [18]. For Ti-6Al-4V, DB is usually conducted at 900 to 950 ^{o}C, tens of degrees lower than the β transus temperature (~ 990 ^{o}C) [17]. To prevent any distinct transformation in SCLR, a TTT diagram for $Zr_{52.5}Al_{10}Cu_{15}Ni_{10}Be_{12.5}$ is measured in a temperature range of 455 ^{o}C to 485 ^{o}C, with intervals of 5 ^{o}C. The sample is heated to a certain temperature within the range, and held until the crystallization occurs. The crystallization time, t_xs, are labeled by downward arrows in Fig.2a. As shown by the TTT diagram (the inset in Fig.2a), t_x increases with the annealing temperature decrease, and it extends to 94 minutes when the temperature reduces to 455 ^{o}C (see Fig.2a). By extrapolating the trend exhibited in the TTT diagram, we notice that the t_x for $Zr_{52.5}Al_{10}Cu_{15}Ni_{10}Be_{12.5}$ below 450 ^{o}C should be no less than 100 min. As a result, the DB experiments in this work are conducted at 440, 435, 430, 425, 420, 415 and 410 ^{o}C, respectively.

In a DB process, a sufficient pressure must be applied to bring the mating surfaces into intimate contact [17]. Once the sheets touch, the pressure forces the surface asperity creep and the contact area increase. Meanwhile, the pressure drives the material in bulk to break through the interfacial oxide film and form a bonding

contact on the atomic scale [11]. Suh et al. found the plastic zone size decreases from 718 μm in as-cast $Zr_{44}Ti_{11}Cu_{20}Be_{25}$ (Tg=340 ^{o}C) to 259 μm in the same alloy annealed for 120 min at 350 ^{o}C [19]. In $Zr_{41}Ti_{14}Cu_{12.5}Ni_{10}Be_{22.5}$, the fractograph changes from the vein pattern associated with localized plastic flow in an as-cast sample to a river pattern associated with cleavage fracture in an annealed sample [14]. This indicates that annealing in SCLR can reduce the toughness of BMGs dramatically, which is usually attributed to structural relaxation or free volume annihilation through atomic diffusion and rearrangement [20]. As a result, if the bonding temperature is fixed, it is logically reasonable to increase the bonding pressure to shorten the bonding time in order to prevent structural relaxation. Under an applied pressure of 200 MPa for 10 min, the $Zr_{65}Cu_{15}Ni_{10}Al_{10}$ was successfully bonded without intervening crystallization [12]. Similarly, Yamaura et al. used a pressure up to 211 MPa for 5 min in the bonding of a metallic glass ribbon and SUS316L porous filter, and they found a sound bonding formed and that the bonding strength increased with the pressure [21]. This suggests a pressure of ~ 10^2 MPa is necessary. Therefore, 100 MPa and 150 MPa are applied in this work.

Bonding time is also important. How the pressure affects t_x in the TTT diagram for BMGs is unknown so far due to the lack of an experimental database, hence the bonding-time determination is not a straightforward task. In austenite to martensite transformation of steel, an externally applied stress can lower the nucleation barrier for coherency loss of second phase precipitates, therefore aiding the martensite nucleation; a hydrostatic compression, however, can stabilize the austenite (fcc) with a smaller atomic volume, hinder the transformation to martensite (bcc) thanks to the volume expansion [22]. As known, BMGs contract ~ 1% in specific volume if crystallized [5], and pressure reasonably favors the contraction. In other words, the pressure can lower the activation energy for structural relaxation of BMG and make the C-shaped curve in the TTT diagram shift left to a shorter time. Accordingly, to prevent any crystallization and to alleviate the structural relaxation as much as possible, the holding time in SCLR is taken to be 10 and 15 min in this work, one order of magnitude shorter than the corresponding t_x (> 100 min) in the TTT diagram

(see Fig.2a). In addition, to heat the sample rapidly and homogeneously within a shorter time, the resistance heating method, which takes advantage of ohmic dissipation, is adopted [23]. The convectional heating method, like heating elements, supplies heat through the boundary of the sample, so the temperature gradient exists at the beginning due to heat conduction and it will take tens of seconds to establish a uniform temperature distribution. Conversely, the resistance heating method dissipates the power volumetrically so that the temperature rises quickly and homogeneously throughout the sample, which benefits the processing of BMGs at an elevated temperature. The three main bonding parameters, i.e., temperature, pressure and time are listed in Table I, as well as the bonding results.

3. Results and discussion

3.1Bonding results

As listed in Table I, specimens A1 to E2 are successfully bonded, but bonding of F1 to G1 is unsuccessful. Fig.3(a) shows the temperature-time dependence of the DB for three bonded sample B1, B4 and C3 when the load is constant. The initial bonding pressure, e.g. for B1, is 150 MPa. When the temperature increases, the two pressing platens and BMG sheets (see Fig.1) begin to thermally expand. The expansion is compensated at ~ 384 ^{o}C by the reduction of the thickness of the sample due to the lateral flow of material. Interestingly, the compensation temperature for B4, under a pressure of 100 MPa, is also ~ 384 ^{o}C. The Newtonian flow strength is given by $\sigma_{flow} = 3\dot{\varepsilon}\eta$ where $\dot{\varepsilon}$ is strain rate and η is viscosity[25]. For B4, as shown in Fig.3(a), the flow process is basically finished within 2 min (see details between the two vertical dashed lines), so σ_{flow} is calculated to be 10^1~10^2 MPa [26]. For B1, despite a larger applied pressure (150 MPa), the flow process is also nearly completed within 2 min, as manifested by the red curve in Fig.3(a). This demonstrates that the viscous flow in MGs is not sensitive to a pressure in excess of 100 MPa. Nevertheless, it is very sensitive to temperature [27]. For C3 at a processing temperature 5 ^{o}C lower than B1 and B4, the viscous flow continues until the end of

bonding process (see the blue curve in Fig.3(a)). It is worthwhile to note that DB is not a flow process in nature but a diffusion one which is substantially associated with to the metallurgical bonding [17]. In DB of Ti-6Al-4V, a bonding time of ~ 2 hours is necessarily needed for atoms to diffuse to recrystallize across the original interface [17]. In DB of BMGs, however, crystallization must be avoided, so the bonding time is reduced to about ten minutes [21]. On the other hand, diffusion behaviors in metallic glasses are divided into two different Arrhenius regions below and above a "kink temperature", i.e., T_g [28]. Although the diffusion coefficient $D=D_o\exp(-H/k_BT)$ in which D_o, H, k_B, and T are pre-exponential factor, activation enthalpy, Boltzmann's constant, and temperature, respectively, holds in both regions, D_o and H are higher for the SCLR than for glass state [28]. A relatively lower bonding temperature Ts for F1 to G1 greatly reduces their Ds. Because of the smaller Ds, the interfacial void shrinkage proceeds slowly, and atom-to-atom bonding does not form in the contact area within the holding time, which eventually results in the bonding failure. On the contrary, the diffusion progresses adequately in sample A1 as no visible interface line can be detected in the polished cross section, as shown in Fig.2b (those for A2 to E2 are similar but not shown here). The glassy state of all bonded samples is maintained, verified by the XRD patterns in Fig.3c (only samples A1, B1, C3 and D3 shown here and others not). Furthermore, to check the bonding interface quality, the same sample in Fig.3b was immersed in 3 N HCl solution for 18 hours, after which the pitting spots is uniformly distributed everywhere on the cross section and no preferential corrosion was observed around the middle line (which is expected to be the interface line), as shown in Fig.3d. This demonstrates that a strong metallurgical bonding is achieved.

3.2 Bending behaviors

Some of bonded samples were three-point bended. Unfortunately, samples A1 to A4 are severely embrittled, and they all break into pieces when prepared for the bending experiments. The flexural stress-strain curves of typical samples B1, B4, C3, D3 and E3 are displayed in Fig.4. An as-cast sample (Ac hereafter) is also bended for comparison purposes. According to the ASTM D790, the flexural stress σ_{fl} and

flexural strain ε_{fl} are given by $\sigma_{fl}=3PL/2wb^2$, $\varepsilon_{fl}=6db/L^2$ for a rectangular cross section, where P is the bending load, L is the support span, d is the bending displacement at the middle point of the sample, and w, b are the width and thickness of the sample, respectively [29]. The curve for Ac deviates from the elastic linearity at about 2.3 GPa. After ~ 5.5% flexural strain, σ_{fl} approaches a maximum value of 2.77 GPa. Ac ruptures when ε_{fl} reaches 6.9%. In sharp contrast, B1 ruptures brittly at 1.51 GPa, which proves B1 is undermined not only on toughness but also strength. A similar situation occurs to B4, but it has a flexural sstrength 2.48 GPa, much higher than that of B1. In DB of $Zr_{65}Al_{10}Ni_{10}Cu_{15}$, Somekawa et al. found that a pressure change from 150 MPa to 200 MPa had little effect on the lap strength of the bonded sample [12]. So it is the longer holding time in SCLR that weakens the mechanical performance to a certain degree. C3, however, sustains a flexural stress up to ~ 3.0 GPa before departure from a linear elastic response to the load. At first time, C3 is unloaded when the applied stress increases to 3.30 GPa, as shown by the orange curve C3a in Fig.4. Then C3 is investigated using microscope, with no obvious deflection observed. More importantly, no shear banding, considered as the principal mechinism for the plastic deformation of MGs, is found on the surface of C3. Afterwards, C3 is reloaded until the failure takes place at 3.35 GPa, as shown by the red curve. Obviously, it has a much higher flexural strength than Ac, but no any plasticity is obtained. The flexural property of D3 bonded at 425 ^{o}C is very similar to that of C3. When the bonding temperature goes down to 420 ^{o}C, close to T_g=416 ^{o}C, σ_{fl} for the E1 approaches that for Ac. But the E1 also fractures in a brittle way like C3, which undergoes a significantly smaller ε_{fl} than Ac. Consequently, as far as the flexural performance is concerned, the diffusion bonding of $Zr_{52.5}Al_{10}Cu_{15}Ni_{10}Be_{12.5}$ in its SCLR should be conducted at 420 to 435 ^{o}C under a pressure of ~ 10^2 MPa within 15 min.

3.3 Fracture morphologies

To understand the distinguishable influences of the bonding process with various operating parameters on the mechanical performance of bonded samples, the fracture behaviors of B1, B4, C3, D3 and E1 are investigated by SEM, and two typical results

(for B1 and C3) are presented here. For comparison, the fractured Ac is also checked. Fig.5a shows a side view of Ac. Clearly, a few shear bands (SBs), marked by arrows, have developed near the fracture surface. There are not only primary SBs (marked by the two white arrows) but secondary SBs (marked by the two black arrows), and they interact with each other (see details in the regions near the end point of the black arrow). This suggests that a moderate plasticity can be measured in the as-cast $Zr_{52.5}Al_{10}Cu_{15}Ni_{10}Be_{12.5}$ by three-point bending [30], which is consistent with the flexural strain-stress result in Fig4a. Conversely, B1 doesn't show any hint of plastic deformability in that no SBs can be found on the side near the fracture, as can be seen in Fig4b. Instead, a crack is formed, as marked by the arrow. One can see the two new fracture surfaces inside the crack are smooth like cleavage plane. Either vein patterns or melting droplets, which, as an indicator of toughness [31], are often noticed on the fracture surfaces of as-cast Zr-based MGs, are not detected at all. Logically, B1 is brittle at least on the macro-scale, confirmed by its response to the bending load (see Fig.3). Interestingly, some regions (marked by black arrows) are relatively rougher than others (marked by white arrows) on the fracture surface in Fig.5c. Looking into the rough region enclosed by the solid line with a large magnification (see Fig.5d), we find a sub-feature in which the rough zone (marked by a black arrow) and the smooth zone (marked by a black arrow) appear alternatively. Actually, an dimple structure seems to be observed in the rough zone using a higher magnification as marked by black arrow in Fig.5e, and the plastic process zone size should be less than1 μm [32]. It means that B1 is as brittle as Mg- or Fe- based MGs which often break in an explosive way. Interestingly, a bonding interface line is unambiguously discovered in the fractograph, even though it is not visible in Fig.3b and Fig.3d. It goes by the end points of the two arrows in Fig.5d and keeps straight, indicating the joining is of metallurgical nature not an anchoring effect. More interestingly, the morphologies across the line is the same and no debonding occurs (see the zone marked by the white arrow in Fig.5e). It proves that the interface hardly affects the fracture behavior of B1 and the brittleness introduced during the bonding process is not caused by the interface but by the annealing effect [4,19].

Figure 6 shows the fracture characteristics of C3. A side view in the vicinity of fracture is presented in Fig.6a. Apparently, no shearing events occur in C3 like the situation in B1. There is no feature of SBs even with a larger magnification, as shown in Fig.6b corresponding to the region enclosed by dotted line in Fig.6a. Without doubt, the defection of C3 in the bending test (see the curve in Fig.3) is fully elastic and never involves plasticity. More significantly, the debonding, excluded in B1, occurs in C3 after failure. One can see an microcrack marked by the arrow in Fig.6b, but the crack does not propagate deeply into the sample. The crack tip opening displacement is much less than 1μm, so the bonding interface hardly causes the stress concentration [24]. Of course, the debonding, which results in premature failure of the bonded material, is not expected in DB. For C3, however, the flexural strength is remarkably higher than that for the as-cast $Zr_{52.5}Al_{10}Cu_{15}Ni_{10}Be_{12.5}$ as described above. It indicates that the debonding stress in C3 exceeds the intrinsic strength of the original material. In this case, the debonding, compared with the embrittlement, may not be a main concern any longer. Fig.6c gives an overall image of the fracture surface for C3. A clearly visible bonding line, tangent to the three dotted circles, goes through the whole sample in the middle, and the morphologies across the bonding line are strikingly different. The region marked by the three circles looks like a radial pattern which is usually considered as the originating site for the crack. This is significantly different from that for B1 in which no debonding takes place.

3.4 Processing window of DB

Although the model for DB was developed in crystalline solids by Pilling and Hamilton [17], there is a substantial difficulty in predicting and controlling the quality of the bonding and the performance of the bonded components due to the process variation. In the DB of BMGs, it becomes more difficult in that MGs are thermodynamically metastable and the structural relaxation cannot be avoided entirely. In principle, DB is just to join the separate materials through volume diffusion while guaranteeing that the properties of the bonded sheet are the same as those of the parent materials [17]. In practice, it's virtually impossible. After the

micron sized pores at the bonding interface shrink to nano-voids under an applied pressure at an elevated temperature, the bonding is to be completed through nano-voids diffusion out of the sample [17]. The recrystallization then proceeds, and the new grains are shared at the interface. Meanwhile, the grains grow coarse and the structure transforms. Hence, the DB joints are inferior to the parent materials in shear, peel, and Charpy impact tests [33]. The metastable nature complicates the evolution regarding the microstructure and performance in the MGs. Still, the DB can be understood from two aspects. While the nano-voids at the interface are slowly diffusing outside the bulk, the atom-to-atom bonding across the interface is gradually formed. At the same time, voids sized on the atomic scale, the so-called free volume, are annihilated, leading to the increase of the critical stress level to activate the shear transformation zone or shear flow unit. The plastic deformation by virtue of shearing is therefore suppressed. On the other hand, experimental evidence reveals that the glass transition is shifted to a slightly higher temperature in annealed MGs compared with the as-cast ones [34]. The fracture stress of MGs is proportional to T_g [35]. Therefore, the annealed MG fractures under a higher stress but in a brittle way. This explains the behaviors of C3. In order to eliminate the bonding interface as much as possible, a higher bonding temperature or/and a longer bonding time must be programmed. If so, the free volume in MG will be exhausted to an equilibrium value, making the MG more brittle. Both strength and deformability of brittle solids are very sensitive to defects such as pores or microcracks which always cause stress concentrations. Unfortunately, the pores and microcracks cannot be excluded in casting and machining procedures. Thus B1 fractures in a brittle fashion prior to yielding under a stress much less than the strength of the parent alloy.

It should be emphasized that the parameters in favor of the DB process are not always beneficial to the performance of the bonded materials. It holds true for crystalline alloys like Ti-6Al-4V and MGs. On the one hand, diffusion promotes the metallurgical bonding; on the other hand, it changes the properties of the parent materials. A balance between the two aspects needs to be realized. Apparently, the bonding parameters for C3 are close to the balance, while those for B1 are not.

Accordingly, the temperature, time and pressure windows for the bonding will be all squeezed when the interrelationship between the three parameters and the microstructure evolution in MGs is taken into account. They are even likely to be closed if other properties, e.g. magnetism, are additionally of concerned. So, the range of temperature-pressure-time combinations determines whether the DB can indeed be completed and the performance of the bonded materials can meet the in need engineering requirement.

4. Conclusions

A study on the phenomenology of diffusion bonding in a bulk metallic glass of $Zr_{52.5}Al_{10}Cu_{15}Ni_{10}Be_{12.5}$ in its supercooled liquid region has been undertaken. When sufficient pressure and time are adopted, the temperature is a key factor for the success of the bonding process. The flexural performance of the bonded samples is assessed in three-point bending tests. The combined influences of temperature, time and pressure applied in DBs on the performance of the bonded BMGs are understood in view of the relationship between the three parameters and the structure evolution. The concluding remarks for the investigation are:

1. The metallic glass $Zr_{52.5}Al_{10}Cu_{15}Ni_{10}Be_{12.5}$ can be bonded by diffusion without crystallization in its SCLR in the temperature range from 420 to 440 ^{o}C, the pressure between 100 and 150 MPa and a time of about 10 min;

2. The performance of the bonded samples is dependent on not only the coalescence of the contacting surfaces but also the rearrangement of atoms inside bulk;

3. The range of temperature-pressure-time combinations settles the probability of success in DB, and the optimization can fulfill the potential for such bonded materials.

Acknowledgements

The work described in this paper was supported by a grant from the Research Grants Council of the Hong Kong Special Administrative Region, China (Project No.: PolyU

511510). The financial support from the NSF of China (Grant No. 51201001) is also appreciated.

References

[1] Klement W, Willens RH, Duwez P. Nature 1960;187:869-70.
[2] Johnson WL. MRS Bulletin 1999;24:42-56.
[3] Inoue A, Takeuchi A. Mater Trans JIM 2002;43: 1892-906.
[4] Schroers J. Adv Mater 2009;21:1-32.
[5] Wang WH. Prog Mater Sci 2012;57: 487-656.
[6] Chen HS, Miller CE. Rev Sci Instrum 1970;41:1237-8.
[7] Conner RD, Johnson WL, Paton NE, Nix WD. J Appl Phys 2003;94:904-11.
[8] Egami T. Rep Prog Phys 1984;47:1601-725.
[9] Wu WF, Li Y, Schuh CA. Philo Mag 2008;88:71-89.
[10] Wiest A, et al. Scripta Mater 2009;60:160-3.
[11] Kawamura Y. Mater Sci Eng A 2004;375-377: 112-9.
[12] Somekawa H, Inoue A, Higashi K. Scripta Mater 2004;50:1395-9.
[13] Kawahito Y, et al. Mater Sci Eng B 2008;148:105-9.
[14] Lewandowski JJ, Wang WH, Greer AL. Philo Mag Lett 2005;85:77-87.
[15] Kuo PH, et al. Mater Chem Phys 2010;120:532-6.
[16] Xiao X, et al. J All Comp 2003;351: 324-8.
[17] Sanders DG, Ramulu M. J Mater Eng Perf 2004;13:744-52.
[18] Nicholas MG. Joining Process, Kluwer Academic Publishers, The Netherlands, 1998.
[19] Suh JY, et al. J Mater Res 2010;25:982-90.
[20] Wang JG, et al. Scritpa Mater 2010;62: 477-482.
[21] Yamaura S, Kimura H, Inoue A. Mater Trans JIM 2007;48, 273-6.
[22] Porter DA, Easterling KE. Phase Transformations in Metals and Alloys, Chapman & Hall, London, 2nd ed. Chap.6 1992.
[23] Johnson WL, et al. Science 2011;332: 828-33.
[24] Schuh CA, Hufnagel TC, Ramamurty U. Acta Mater 2007;55: 4067-109.
[25] Schroers J. Scripta Mater 2007;57: 341-4.
[26] Johnson WL, Demetriou MD, Harmon JS, Lind ML, Samwer K. MRS Bulletin 2007;32:644-50.
[27] Schroers J. Acta Mater 2008;56: 471-8.
[28] Faupel F, et al. Rev Mod Phys 2003;75:237-80.
[29] ASTM D790. Test methods for flexural properties of unreinforced and reinforced plastics and electrical insulating materials, in Annual Book of ASTM Standards, Vol. 08.01 ASTM International,West Conshohocken, PA, 2003.
[30] Schroers J, Johnson WL. Phys Rev Lett 2004;93:255506.
[31] Jiang M Q, Dai LH. Phil Mag Lett 2010;90:269-77.
[32] Xi XK, et al. Phys Rev Lett 2005;94:125510.

[33] Carrión JG. RTO AVT Specialists' Meeting on "Cost Effective Application of Titanium Alloys in Military Platforms", held in Loen, Norway, RTO-MP-069(II), 7-11 May 2001.
[34] Suryanarayana C, Inoue A. Bulk metallic glasses, chapter 5. USA:Taylor and Francis Group LLC; 2011.
[35] Yang B, Liu CT, Nieh TG. Appl Phys Lett 2006;88 :221911.

Figure Captions

Figure 1. A schematic sketch of the DB setup. Two loaded BMG sheets are heated by ohmic heating and cooled by cutting off the electricity and introducing pure argon. The temperature is monitored by a thermocouple (TC).

Figure 2. Isothermal annealing in the temperature range of 455 ^{o}C to 485 ^{o}C with intervals of 5 ^{o}C using DSC. Inset is the TTT diagram for the $Zr_{52.5}Al_{10}Cu_{15}Ni_{10}Be_{12.5}$.

Figure 3. The DB processes and results of typical samples. (a) The displacement (colored curves) of the pressing platen and the bonding temperature (black curve) with time in the DB process under a constant load. The temperature at P is 384 ^{o}C. (b) A featureless SEM observation of the polished cross section of the bonded sample A1. (c) The XRD patterns of A1, B1, C3 and D3. (d) A SEM micrograph of A1 immersed in 3 N HCl for 18 hours and the yellow dotted line supposed to the bonding interface line.

Figure 4. The flexural performances of the bonded samples B1, B4, C3, D3, and E1 as well as the as-cast one.

Figure 5. SEM observations on the fracture behavior of Ac and B1. (a) The side view of ruptured Ac undergoing a plastic deflection where multiple shear bands can be seen as marked arrows. (b) A side view of ruptured B1 where no shear bands can be found but a crack has developed as marked by the arrow. (c) An overall SEM fractograph of B1 on which appear smooth regions marked by white arrows and rough regions marked by black arrows. (d) A magnified image of the region enclosed by the solid line in (c), showing the bonding interface line going through the end points of the two arrows. (e) A magnified image corresponding to the region marked by the white arrow in (d), exhibiting a smooth surface marked by the white arrow and a dimple structure with a size much less than 1μm as marked by the black arrow.

Figure 6. SEM observations on the fracture behavior of C3. (a) A side view near the fracture surface of ruptured C3. (b) A magnified image corresponding to the region enclosed by the dotted line in (a) where the debonding occurs as marked by the arrow. (c) An overall image of the fracture surface of C3, showing the bonding interface line tangent to three dotted circles which enclose the originating sites of the crack.

Table Caption

Table I. Experimental data of bonding parameters, i.e., temperature, time, and pressure used in DB of $Zr_{52.5}Al_{10}Cu_{15}Ni_{10}Be_{12.5}$ and the results of DB (S means success and F means failure).

Table(s)

Table I. Experimental data of bonding parameters, i.e., temperature, time, and pressure used in DB of $Zr_{52.5}Al_{10}Cu_{15}Ni_{10}Be_{12.5}$ and the results of DB (S means success and F means failure).

No	Temperature (^{o}C)	Pressure (MPa)	Time (min)	S/F
A1	440	150	15	S
A2	440	150	10	S
A3	440	100	15	S
A4	440	100	10	S
B1	435	150	15	S
B2	435	150	10	S
B3	435	100	15	S
B4	435	100	10	S
C1	430	150	15	S
C2	430	150	10	S
C3	430	100	15	S
C4	430	100	10	S
D1	425	150	15	S
D2	425	150	10	S
D3	425	100	15	S
D4	425	100	10	S
E1	420	150	15	S
E2	420	150	10	S
F1	415	150	15	F
F2	415	150	10	F
G1	410	150	15	F

Figure 1

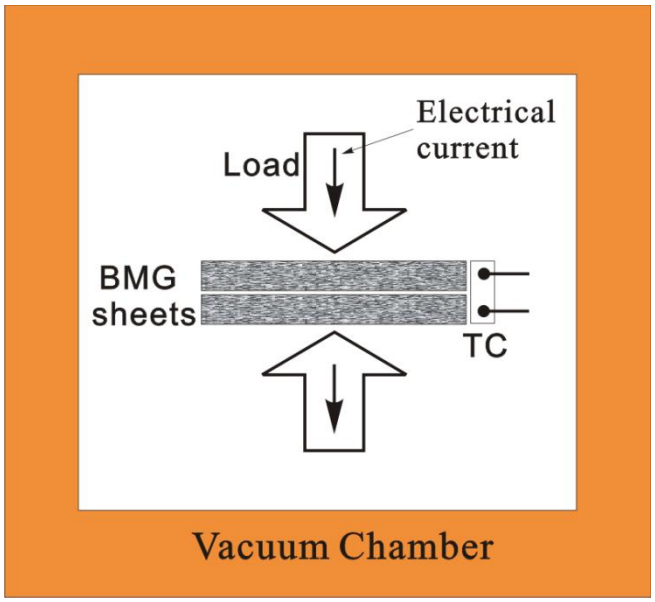

Figure 1. Wang et al.

Figure 2

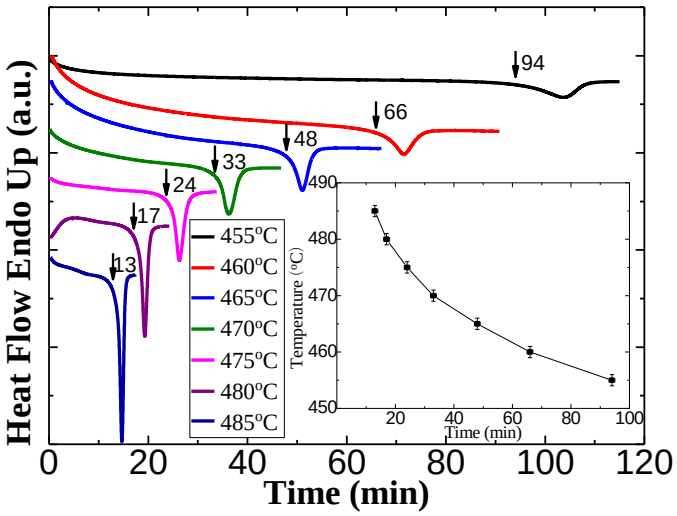

Figure 2. Wang et al.

Figure 3

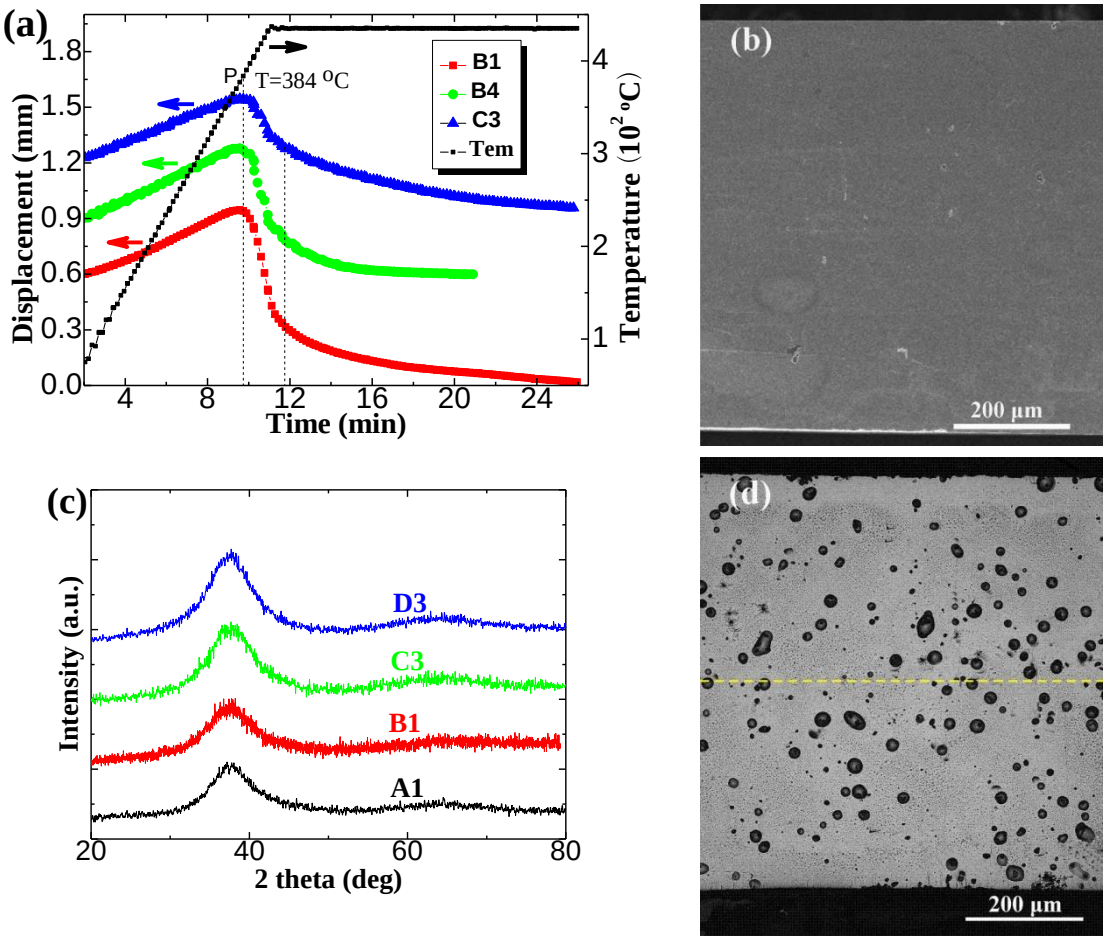

Figure 3. Wang et al.

Figure 4

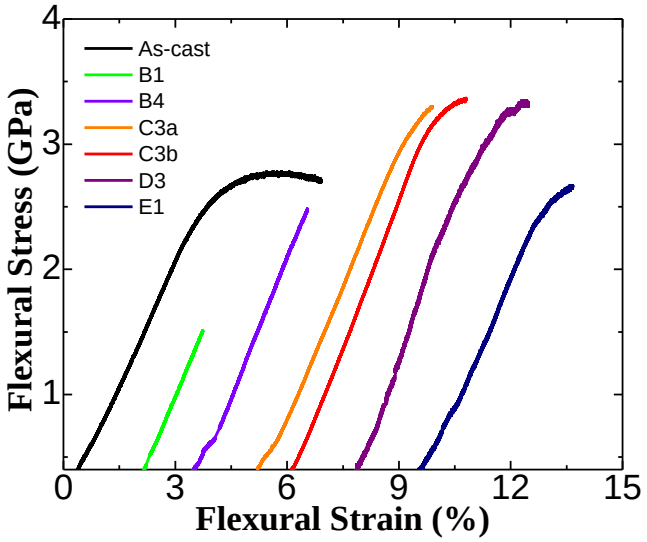

Figure 4. Wang et al.

Figure 5

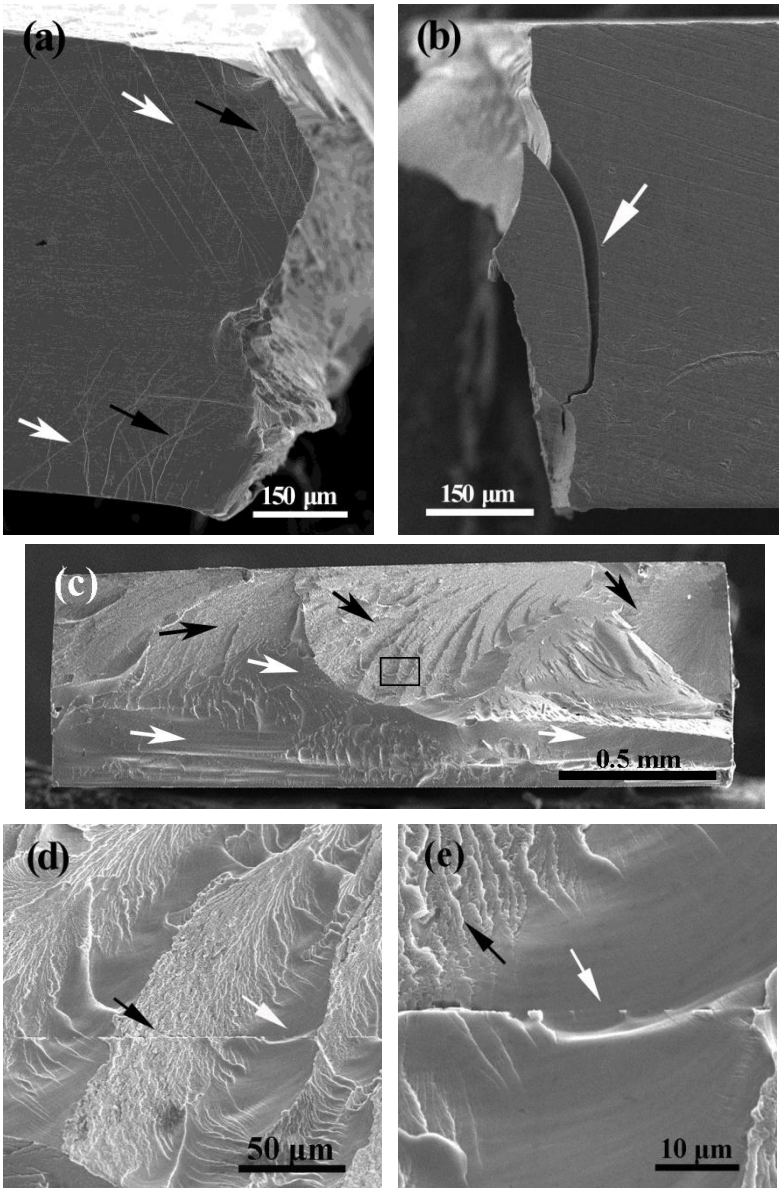

Figure 5. Wang et al.

Figure 6

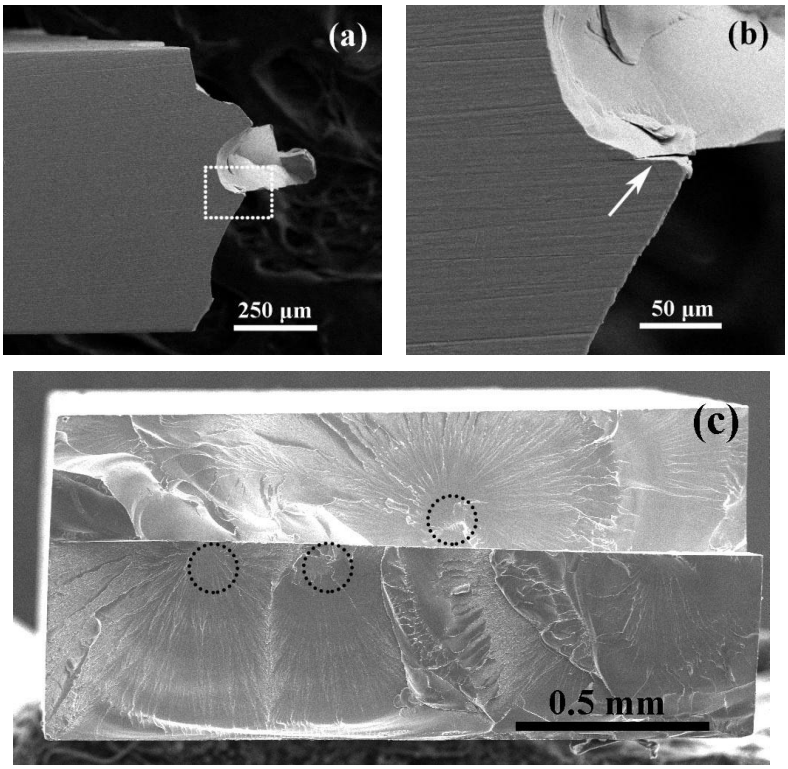

Figure 6. Wang et al.